J. Am. Soc. Mass Spectrom. (2018) 29:342–351
DOI: 10.1007/s13361-017-1841-6

FOCUS: 32nd ASILOMAR CONFERENCE,
NOVEL INSTRUMENTATION IN MS AND ION MOBILITY: RESEARCH ARTICLE

A Hybrid Constant and Oscillatory Field Ion Mobility Analyzer Using Structures for Lossless Ion Manipulations

Aneesh Prabhakaran, Ahmed M. Hamid, Sandilya V. B. Garimella, Blandina R. Valenzuela, Robert G. Ewing, Yehia M. Ibrahim, Richard D. Smith

Biological Sciences Division, Pacific Northwest National Laboratory, Richland, WA 99352, USA

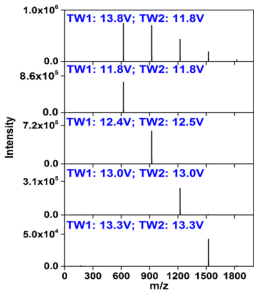

Abstract. Here we explore the combination of constant and oscillatory fields applied in a single device to affect the continuous separation and filtering of ions based on their mobilities. The device explored allows confining and manipulating ions utilizing a combination of radio frequency (rf), direct current (DC) fields, and traveling waves (TW) in a structures for lossless ion manipulations (SLIM) module. We have investigated theoretically and experimentally a concept for continuous filtering of ions based on their mobilities where ions are mobility separated and selected by passage through two regions, both of which incorporated combined TW and constant fields providing opposing forces on the ions. The SLIM module was composed of two surfaces with mirror-image arrays of electrodes and had two regions where the different TW and opposing DC fields could be applied. The filtering capabilities are determined by the applied DC gradient and the TW parameters, such as speed, amplitude, and the TW sequence (i.e., the duty cycle of the traveling wave). The effects of different parameters on the sensitivity and the ion mobility (IM) resolution of the device have been investigated. By appropriately choosing the DC gradient and TW parameters for the two sections, it is possible to transmit ions of a selected mobility while filtering out others of both higher and lower mobility. The novel device described here provides a basis for the targeted analysis of compounds based upon the continuous selection of ions according to their mobility and without the need for high electric fields or pulsed injection.

Keywords: Ion mobility, Traveling wave, Constant field, Ion filter, SLIM

Received: 31 May 2017/Revised: 25 October 2017/Accepted: 30 October 2017/Published Online: 12 December 2017

Introduction

The ability to identify molecular species in samples depends on the nature of the techniques that distinguish molecules based upon their physical and chemical properties. Ion mobility (IM) spectrometry has increasingly become an important technique in conjunction with MS for analysis based on ion size or shape. IM has been utilized in a variety of applications such as the detection of warfare agents, explosives, biological agents, and drugs, etc. [1–4]. IM-based instruments are widely used in e.g., airports and seaports working as 'artificial noses' to detect specific markers [5, 6], and IM-MS is increasingly used for a wide range of analytical applications because of the complementary information provided [7–13]. Separating ions in IM relies on a balance between the forces from the electric field and drag resulting from the buffer gas, providing the basis for an array of IM approaches, including drift tube IM (DTIM) [14], traveling wave IM (TWIM) [15], differential mobility analyzers (DMA) [16], etc. [17–24]. Some of these IM approaches are used at atmospheric pressure (e.g., DTIM and DMA) whereas others are used at low pressure to facilitate coupling with MS. In the classic drift tube IM, the forces due to the constant field and collisions with the buffer gas primarily dictate ion motion. Ions of lower mobility collide more frequently with the buffer gas molecules/atoms. In trapped IM, ions are separated based on a balance between the flow of gas and the opposing constant field [17]; as the field is ramped, while the gas velocity is constant, ions exit the device as a function of their mobility. In TWIM, ions either 'keep up' with a constantly moving wave (i.e., an oscillatory field) or are

Aneesh Prabhakaran and Ahmed M. Hamid contributed equally to this work.

Electronic supplementary material The online version of this article (https://doi.org/10.1007/s13361-017-1841-6) contains supplementary material, which is available to authorized users.

Correspondence to: Yehia Ibrahim; *e-mail:* yehia.ibrahim@pnnl.gov, Richard Smith; *e-mail:* rds@pnnl.gov

'passed over' by the TW in a mobility-dependent fashion to effect the separation [25, 26]. For instance, ions of low mobility tend to fall behind more often as the wave moves past them, whereas ions of higher mobility tend to keep up with the wave and fall behind less often. Each IM approach provides somewhat distinctive design or measurement features.

In this context, structures for lossless ion manipulations (SLIM), a new class of ion optic devices, have enabled a variety of complex gas-phase ion manipulations [27], including lossless ion transmission over a wide *m/z* range, efficient trapping for as long as 5 h, accumulation with near 100% efficiency, execution of 90° turns, and switching to alternative paths [28–35]. SLIM utilize arrays of electrodes patterned on two surfaces arranged parallel to each other, with ions confined between the two surfaces by the effective potentials, created by alternating 180° out of phase rf waveforms, and laterally by DC voltages applied to 'guard' electrodes. Ions can be transmitted and separated by mobility in SLIM using either constant or oscillatory fields [31, 34, 36].

In many IM methods, the separation begins with a pulse of ions injected into the device either using a Bradbury Nielsen gate [37] or releasing an accumulated ion population (e.g., in an ion funnel trap [38]) over a short period of time (~ <= 500 μs) prior to separating ions based upon their mobilities. This inherently introduces a limited duty cycle for IM separations [39], and the duty cycle decreases with increasing separation time or increasing mobility range, being separated because of inherent limitations on the size and charge density of the initial ion packet. (An exception to this limitation has recently been developed using SLIM based upon the ability to spatially compress large distributions of separating ions without loss of IM resolution [40]). Thus, a means of improving duty cycle by e.g., utilizing a continuous ion beam is beneficial. A MS analog is the quadrupole mass filter, which generally provides the highest ion utilization efficiency and measurement sensitivity for targeted measurements (e.g., of a specific *m/z* as in MRM measurements) [41, 42]. Alternatively, where a targeted band of mobilities or chemical structures are to be investigated through separations (for example, where a specific mobility range is of an analytical interest, or where a specific chemical structure is being monitored), we would need methods to select a range of mobilities within a continuously injected ion beam containing a wide range of mobilities.

In this work, we explore the separation characteristics of using an oscillatory field (such as a TW) combined with an opposing constant DC field, to enable transmission of a selective range of mobilities (for either a standalone device or in conjunction with other ion manipulation devices such as mass spectrometer). In such a combination of static and dynamic mobilities, the velocity of ions in a buffer gas attributable to the TW and the constant the DC field determines which range of ion mobilities will be transmitted through the device. As the dependence of ion velocity on the mobility and electric field strength is linear in the low field DTIM while it is not linear in TWIM, the integration of these two fields provides a new capability for gas-phase separations. In this work, the development of a hybrid IM device is facilitated using the flexible electrode architecture enabled with SLIM [33, 36]. Here we report on the development and initial application of a new SLIM device that can continuously select and transmit a narrow range of mobilities without the need for the pulsing of ions or the trapping of ions, while also utilizing low electric fields unlike techniques such as FAIMS/DMS and DMA. We also report supportive ion simulations and our initial evaluation of this new device. We anticipate that this new technology will provide the basis for targeted identification of the chemical compounds by filtering out other unwanted chemical species and also eventually (as a future work) as an initial pre-filter device for deeper chemical enquiry of selective population using high resolution IM.

Experimental

Mass Spectrometry

Positive ions were generated by a nano-electrospray ionization (3000 V) using chemically etched emitters. The sample was infused utilizing a syringe pump (Chemyx, Stafford, TX, USA) with a flow rate of 300 nL/min. Ions were introduced into the first stage of vacuum through a 750 μm i.d. stainless steel capillary heated to 140 °C (Figure 1a). After exiting the heated capillary, ions were focused by a high-pressure ion funnel (10 Torr, ~240$V_{p\text{-}p}$ and ~ 966 kHz) to an ion funnel trap (IFT, 1.1 MHz and ~ 160 $V_{p\text{-}p}$) maintained at 3.95 Torr. The IFT was operated in the continuous mode, i.e., no trapping was utilized. Upon exiting the IFT, ions were injected into a 2.0 cm long quadrupole (1.1 MHz and ~180 $V_{p\text{-}p}$), which guided the ions into the SLIM (4 Torr N_2: both quadrupole and SLIM). The net positive pressure gradient between IFT and SLIM prevents neutrals from entering into the SLIM device and also minimizes any gas dynamics effects. After traversing the SLIM device, ions exited the SLIM into an 18 cm long rear ion funnel (830 kHz and ~350 $V_{p\text{-}p}$) with a 16.5 V/cm DC field, which refocuses the radially diffused ions prior to a 2.5 cm long quadrupole (960 kHz and ~340 $V_{p\text{-}p}$) followed by an Agilent 6538 QTOF mass spectrometer equipped with a 1.5 m flight tube (Agilent Technologies, Santa Clara, CA, USA).

SLIM

The SLIM consisted of two mirror-image 30.5 × 7.6 cm surfaces spaced 4.8 mm apart and fabricated using photolithography. Figure 1a shows a schematic presentation of the experimental setup, with the electrodes arrangement shown in Figure 1b. Ions are efficiently confined laterally by the DC potential applied to the guard electrodes (5.0 mm × 3.2 mm), and 180° out of phase rf waveforms (~250 $V_{p\text{-}p}$ at ~900 kHz) are applied to adjacent rung electrodes (5.0 mm × 1.5 mm) creating a pseudopotential confining to ions between the surfaces. In addition to the rf waveforms, TW and DC gradient potentials are co-applied to the rung electrodes. The TW and DC are generated from a power supply that also provided the rf

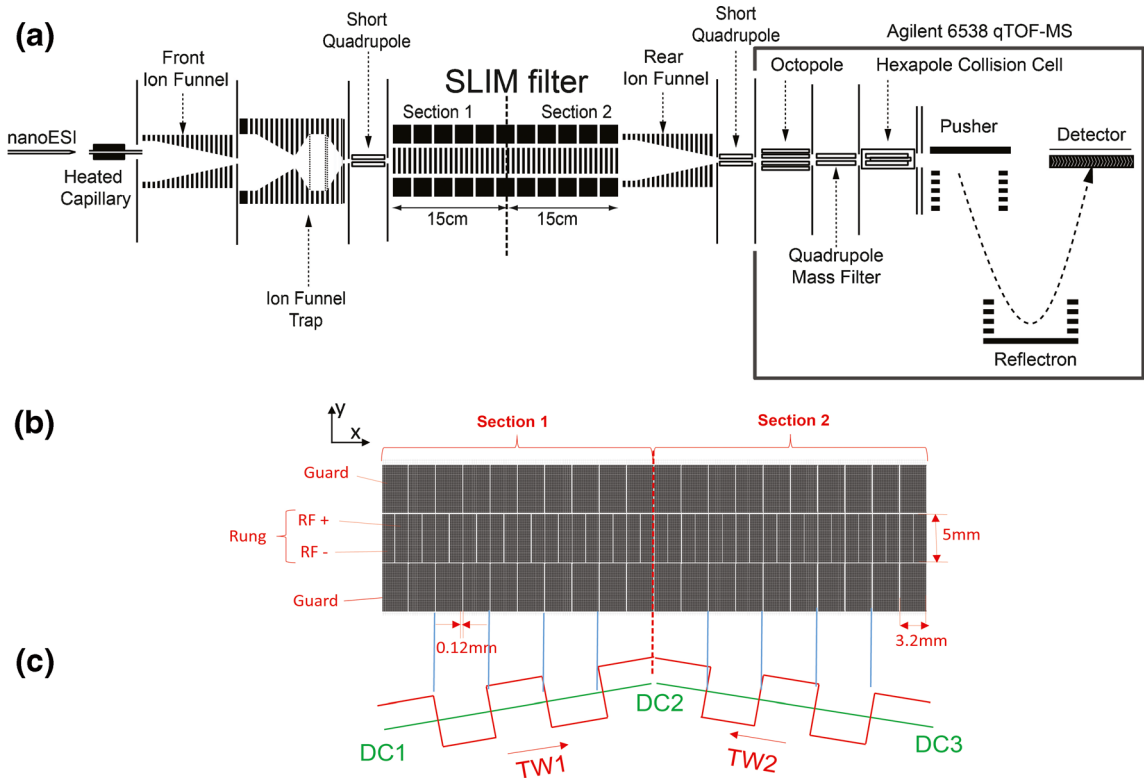

Figure 1. **(a)** Schematic presentation of the experimental arrangement. **(b)** Detailed view of the electrode layout on one of the surfaces. **(c)** Voltage profile that shows the DC gradient (green) on both sections and the traveling wave (red) on both sections. The dashed red line divides sections 1 and 2.

waveforms (GAA Custom Engineering LLC). The speed of the TW is determined by the rate at which the potentials are advanced (i.e., stepped) from one electrode to the next. The SLIM surfaces are divided into two equal sections (Figure 1b) where the TW and DC gradient are both co-applied to each section. Figure 1c illustrates the voltage profile applied to the device where the first and second sections have positive and negative DC gradients, respectively. The DC potential applied to the guard electrodes is also subjected to a corresponding gradient to provide lateral confinement of the ions throughout the device. The DC voltage gradients are established by controlling three independent voltages (at the first, middle, and last electrodes) via resistive chains [28, 33, 35].

The TW was created by switching the DC on and off to individual electrodes of each eight-electrode subset. The TW potentials were applied to a subset (most often four) of the eight electrodes, while the other electrodes of each subset were maintained at ground potential. The TW sequence can be varied between 10000000 and 11111110 where 0 corresponds to –15 V, and 1 corresponds to 15 V, resulting in a peak-to-peak TW amplitude of 30 V to the specified electrode. For example, in a sequence of 11110000, 15 V was applied to electrodes 1–4 whereas a –15 V was applied to electrodes 5–8. The applied voltages were stepped one electrode at a time at a preset speed in the direction of mass spectrometer in the first section and opposite to the direction of the mass spectrometer in the second section.

The balance between the velocity of the ions, attributable to the applied TW and DC gradient, in both sections of the SLIM filter determines the mobility range (i.e., selected ion species) that will be transmitted through the device. The range of mobilities that can be transmitted is varied by adjusting the DC potentials, the TW amplitudes, and TW speeds in both sections. We used ion trajectory simulations (SIMION 8.1) to determine the general range of parameters that would be effective for operating the present device [43]. These simulations used the exact electrode dimensions outlined in the Experimental section, but with a total length of ~10 cm to reduce the computational requirements. The simulations were performed for 100 ions per *m/z* at 4 Torr N_2, the applied DC gradient was ~1.35 V/cm, the guard voltage was maintained 2 V higher than the applied DC voltage to provide lateral confinement of ions, and the TW amplitude used was 12 V. Statistical diffusion simulation (SDS) was used for collisions with the buffer gas [44], and space charge effects were not considered. With simulations for guidance, experimental tuning involved an initial control experiment where a continuous beam is completely transmitted to MS with a unidirectional TW direction towards MS in both SLIM sections. Upon only reversing the TW direction in the second section (located closer to the MS), the ion beam is blocked. By slowly raising the DC potential value at

the interface between the two SLIM sections (DC2 in Figure 1c), a steady gradient is created in the two sections and filtering effect comes into play to eventually obtain a specific range of mobilities depending on the parameters used.

Sample Preparation

Agilent tune mixture and a mixture of nine peptides to provide positive singly charged and multiply charged ions, respectively, were utilized. The nine-peptide mixture was an equimolar mixture of bradykinin acetate salt, kemptide acetate salt, angiotensin I human acetate salt hydrate, angiotensin II human, neurotensin, renin substrate tetradecapeptide porcine, Substance P acetate salt hydrate, melittin from honey bee venom, and fibrinopeptide A human (Sigma-Aldrich, St. Louis, MO, USA). The concentration of the peptides was 100 nM in a buffer of 50/50/1 vol/vol/vol water/methanol/acetic acid (Fisher Scientific, Pittsburgh, PA, USA).

Results and Discussion

In the first section of the present SLIM device the TW moves in the forward direction (positive x-axis direction in Figure 1b), whereas in the second section the TW moves in the reverse direction (negative x-axis direction in Figure 1b). The speed of the TW was varied in each section independently (TW1 and TW2). The transmission of ions through the device is determined by the balance between their velocities attributable to the TW (v_{TW}) and the opposing DC gradient (v_{DC}). The velocity of an ion in the first and second sections attributable to the applied DC gradients can be obtained from Equations 1 and 2, respectively:

$$v_{DC1} = KE_1 \tag{1}$$

$$v_{DC2} = KE_2 \tag{2}$$

while the velocity of the ions attributable to the TW can be obtained from Equations 3 and 4 [45]:

$$v_{TW1} = \frac{\left(K\overline{E}_{TW1}\right)^2}{s_1} \tag{3}$$

$$v_{TW2} = \frac{\left(K\overline{E}_{TW2}\right)^2}{s_2} \tag{4}$$

Here, K is the ion mobility, E_1 and E_2 are the DC gradients applied to the first and second sections, respectively, $\overline{E}_{TW1}$ and $\overline{E}_{TW2}$ are the average electric fields attributable to TW1 and TW2, respectively, and s_1 and s_2 are the speeds of TW1 and TW2, respectively. The condition for ions to pass through the first section of the device is $|v_{TW1}| > |v_{DC1}|$, whereas in the second section the condition for an ion transmission is $|v_{TW2}| < |v_{DC2}|$.Therefore, for a fixed applied DC gradient and length, the resulting velocity attributable to the applied TW in both sections determines whether a specific ion will be transmitted. The following simulations show that the first section provides an effective low mobility cut-off (i.e., only the ions with a mobility greater than a threshold will be transmitted through the first section), whereas the second section will provide a high mobility cut-off (i.e., only ions with mobility less than a threshold will be transmitted). When combined, only a range of mobilities, and potentially a narrow range, will be transmitted through the device.

Our simulations showed that the device can transmit ions according to their mobilities by changing the TW frequencies applied to the two SLIM sections, as illustrated in Figure 2a. To show the ion trajectories, the ion velocities have been extracted from the simulations by recording the time of arrival of ions at a plane defined at a specific distance from the ion starting point and plotted in Figure 2b. The error bar corresponds to the standard deviation of the velocity for the 100 ions simulated for each *m/z* species. The velocities resulting from the DC and TW fields are extracted from the simulations for TW and DC fields independently (i.e., recording the ion velocity attributable to DC gradient while the TW was turned off and recording the ion velocity attributable to TW while DC gradient was switched to zero). As illustrated in Figure 2b, the ion velocities resulting from the applied DC and TW fields are plotted as a function of the reduced mobility of ions, which can be utilized to predict which ions can be successfully transmitted through the device under these conditions. The ion velocity calculations were done for *m/z* 62, 195, 490, 622, 922, 1222, and 1522 ions with corresponding mobilities listed in Table 1. The ion velocities shown in Figure 2b have been calculated by applying DC gradient to the two SLIM sections of 1.34 V/cm and TW frequencies of 180 kHz and 200 kHz to the first and second sections of SLIM, respectively (similar to panel iii in Figure 2a). As the DC gradient is the same on both sections (only the direction changes), the magnitude of the ion velocity due the DC is also same in both sections. Therefore, in Figure 2b, the v_{DC} represents the ion velocity attributable to DC field in both the sections. Under these conditions, it is evident that only *m/z* 62, 195, and 490 and 622 ions will be transmitted through the first section since for these ions $|v_{TW1}| > |v_{DC}|$. In the second section of the device, *m/z* 622, 922, 1222, and 1522 can be transmitted since $|v_{DC}| > |v_{TW2}|$. When both ion velocity plots are combined, only *m/z* 622 will be transmitted. Similarly, by varying the TW parameters and DC gradient, ions of different mobility can be selected for transmission through the device.

Experimental studies were then performed to investigate the effects of the applied DC gradients and TW parameters such as speed, amplitude, and sequence. First, to establish a baseline

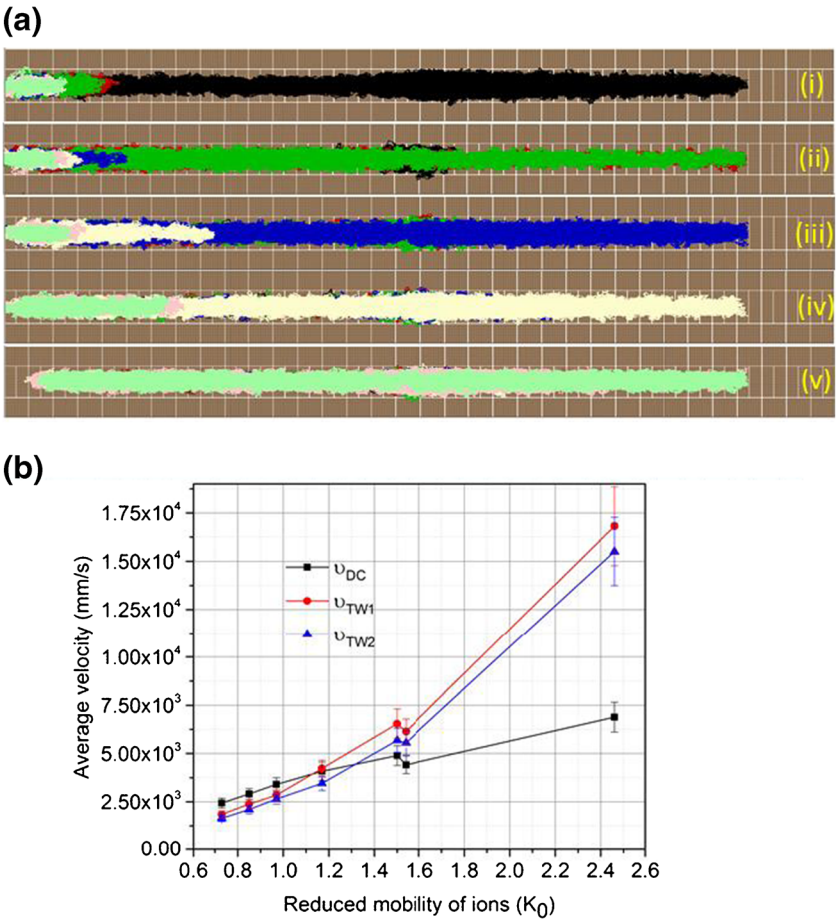

Figure 2. **(a)** A screenshot of the SIMION simulations showing the trajectories of ions of m/z = 62 (black), m/z = 195 (red), m/z = 490 (green), m/z = 622 (blue), m/z = 922 (yellow), m/z = 1222 (pink), and m/z = 1522 (pale green) upon applying a DC gradient of 1.34 V/cm to section 1 and section 2 while the TW speed was varied as follows: (i) TW1 = 456 × 10^3 mm/s, TW2 = 577.6 × 10^3 mm/s; (ii) TW1 = 364.8 × 10^3 mm/s, TW2 = 456 × 10^3 mm/s; (iii) TW1 = 273.6 × 10^3 mm/s, TW2 = 304 × 10^3 mm/s; (iv) TW1 = 228 × 10^3 mm/s, TW2 = 258.4 × 10^3 mm/s; (v) TW1 = 197.6 × 10^3 mm/s, TW2 = 228 × 10^3 mm/s. **(b)** The extracted velocities of ions m/z = 62, m/z = 195, m/z = 490, m/z = 622, m/z = 922, m/z = 1222, and m/z = 1522 as a result of the DC gradient ($|v_{DC}|$) and TW ($|v_{TW}|$) fields in section 1 and in section 2 (Figure2, $v_{DC}$is same in both sections). The applied DC gradient was 1.34 V/cm whereas the TW frequencies applied to section 1 and section 2 were 273.6 × 10^3 and 304 × 10^3 mm/s, respectively. In this case only m/z = 622 passed through the device

reference and to find the optimum DC gradient, a series of mass spectra for Agilent tune mixture were collected at different DC gradients. Figure 3a shows the mass spectrum for Agilent tune mixture ions when the filtering mode was disabled, i.e., a 0 V/cm DC gradient and the TWs applied to the first and second sections (TW1 and TW2) were moving from source to the mass spectrometer. In Figure 3b–f, the direction of TW2 was reversed to move against the ion motion while varying the DC gradient field. At a low DC gradient of 0.9 V/cm (Figure 3b), high mobility ions such as 622 and 922 were not transmitted

Table 1. The mobility values of the peptides composing the nine peptide mixture and Tune mix

Peptides	m/z	Reduced mobility (cm^2 /Vs)	Tune mix species (m/z)	Reduced mobility (cm^2 /Vs)
Fibrinopeptide A	768.9	0.992	62	2.46
Substance P	674.9	1.026	195	1.54
Melittin	712.5	1.075	490	1.50
Angiotensin II	523.8	1.157	622	1.17
Renin	586.9	1.178	922	0.97
Bradykinin	530.8	1.194	1222	0.85
H Neurotensin	558.3	1.234	1522	0.73
H Angiotensin	432.9	1.289		
Kemptide	386.7	1.322		

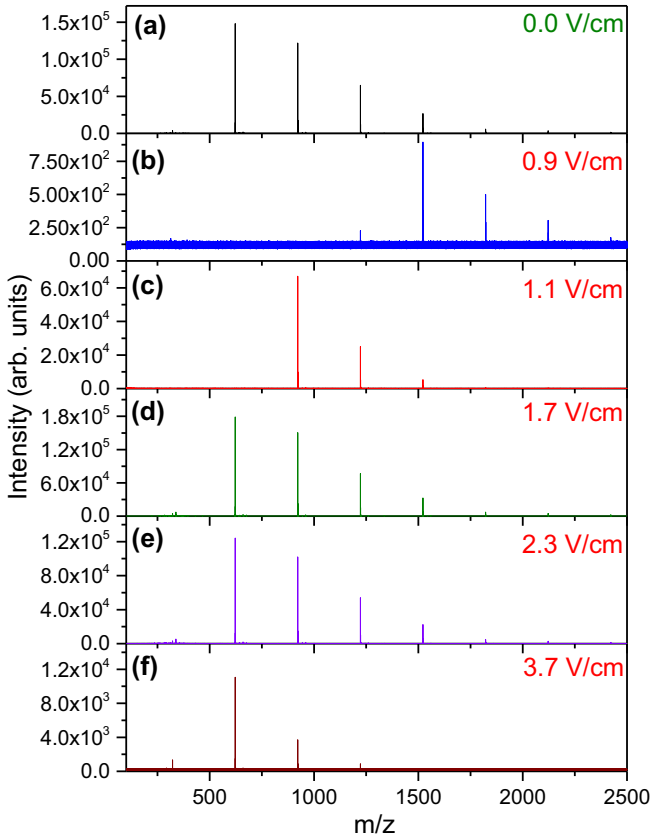

Figure 3. Mass spectra obtained from the analysis of Agilent tuning mixture showing the effect of the DC gradient on both SLIM filter sections. The voltage applied in the middle of the device was raised so that the gradient on both the sections of the filter is increased simultaneously. The TW speed applied to section 1 and section 2 was 74 × 10^3 mm/s and 370 × 10^3 mm/s, respectively. The TW in the first section was forward in all the panels whereas the second TW was moving forward in panel **(a)** whereas moving in the opposing direction in panels **(b–f)**. The TW amplitude was maintained at 12 V

through the device, while the signal for the low mobility ions was also severely limited. This is attributed to the bias against transmission of higher mobility ions through section 2 with this low DC gradient. In contrast, with a high DC gradient, the transmission of the low mobility ions, such as 1222 and 1522, is reduced due to their inability to pass through section 1 (Figure 3e, f). For a DC gradient of 1.7 V/cm (Figure 3d), all ions were transmitted and obtained a spectrum identical to the 0 V/cm gradient and TW in both sections in the same direction (Figure 3a). Therefore, a DC gradient of 1.7 V/cm was chosen for the subsequent experiments.

The effect of TW speed on both sections of the device was studied by keeping all other parameters constant (TW amplitude = 12 V, DC gradient = 1.7 V/cm, and TW sequence = 11110000). As discussed above, only ions whose speed attributable to the TW is higher than that attributable to the DC gradient will pass through the first section, whereas ions with velocities attributable to DC gradient higher than that attributable to the TW will only pass through the second section. Thus, in order to transmit a specific mobility range, both of TW1 and TW2 frequencies need to be tuned while keeping the TW2 speed higher than TW1 speed, assuming that all other parameters are kept constant. Therefore, the frequencies of both TW1 and TW2 were controlled independently in order to transmit specific ion populations. Upon increasing TW1 speed while keeping TW2 speed constant, only higher mobility ions are allowed to pass through the device (Supplementary Information Figure S1a). This can be attributed to the fact that the low mobility ions are more susceptible to a higher number of "rolling over" events and thus are effectively blocked in section 1 while allowing higher mobility ions to pass. In contrast, decreasing TW2 speed while keeping TW1 speed constant resulted in the transmission of lower mobility ions (Supplementary Information Figure S1b), which can be attributed to high mobility ions being blocked in the second section where they experience fewer roll-over events. Therefore, we varied the two TWs frequencies to transmit each of the Agilent tune mixture ions according to their mobilities (Figure 4). The spectrum in black represents lossless transmission of all the major ion species (*m/z* 622–1822). Note that the intensities are normalized to the intensity of *m/z* 622. Figure 4 shows that as the frequencies were set to TW1 = 185 kHz and TW2 = 215 kHz only *m/z* 622 was transmitted (red). As the frequencies were lowered, different ions were transmitted. For instance, *m/z* 922 was transmitted at TW1 = 160 kHz and TW2 = 168 kHz (green) whereas *m/z* 1222 was transmitted at TW1 = 143 and TW2 = 144 kHz (blue). However, ion losses are observed in the course of the filtering process, with the losses more prominent for the lower mobility ions. Losses of 15%, 53%, and 90% in the abundance of *m/z* 622, 922, and 1222, respectively, were observed. We also note from Figure 4 that the lower the mobility to be transmitted, the smaller the difference between TW1 and TW2 frequencies needed. Additionally, for the lower

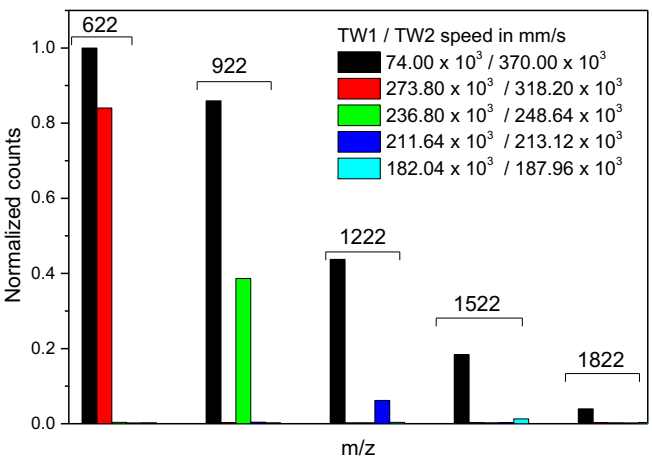

Figure 4. The effect of the TW1 and TW2 speed (mm/s) on the filtering of specific ions from the Agilent tune mixture. Black bars represent mass spectrum collected under conditions where all ions pass through. The red, green, blue, and cyan represent mass spectra under the filtering conditions. TW amplitude and DC gradient were maintained at 12 V and 1.7 V/cm, respectively

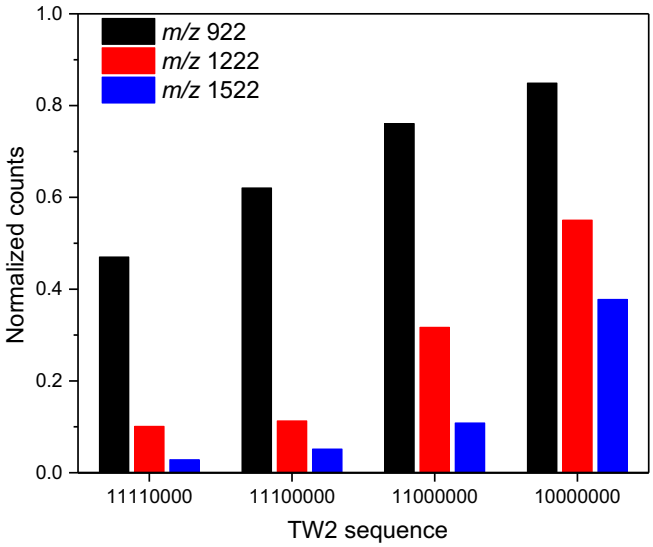

Figure 5. The effect of TW2 sequence (TW1 sequence was maintained 11110000) on the transmission of selected ions. The intensities are normalized to a reference spectrum where all ions were transmitted. The frequencies of TW1 and TW2 were adjusted for the maximum transmission of each ion upon varying TW2 sequence. For the sequence 11110000, the speeds (mm/s) (TW1, TW2) for *m/z* 922 (149.48×10^3, 153.92×10^3), *m/z* 1222 (137.64×10^3, 140.60×10^3), and *m/z* 1522 (119.88×10^3, 122.84×10^3). For the sequence 11100000, the speeds (mm/s) (TW1, TW2) for *m/z* 922 (149.48×10^3, 150.96×10^3), *m/z* 1222 (128.76×10^3, 133.20×10^3), and *m/z* 1522 (112.48×10^3, 113.96×10^3). For the sequence 11000000, the speeds (mm/s) (TW1, TW2) for *m/z* 922 (152.44×10^3, 105.08×10^3), *m/z* 1222 (136.16×10^3, 90.28×10^3), and *m/z* 1522 (118.40×10^3, 79.92×10^3). For the sequence 10000000, the speeds (mm/s) (TW1, TW2) for *m/z* 922 (156.88×10^3, 25.16×10^3), *m/z* 1222 (143.56×10^3, 22.20×10^3), and *m/z* 1522 (133.20×10^3, 20.72×10^3). The TW amplitude was maintained at 12 V

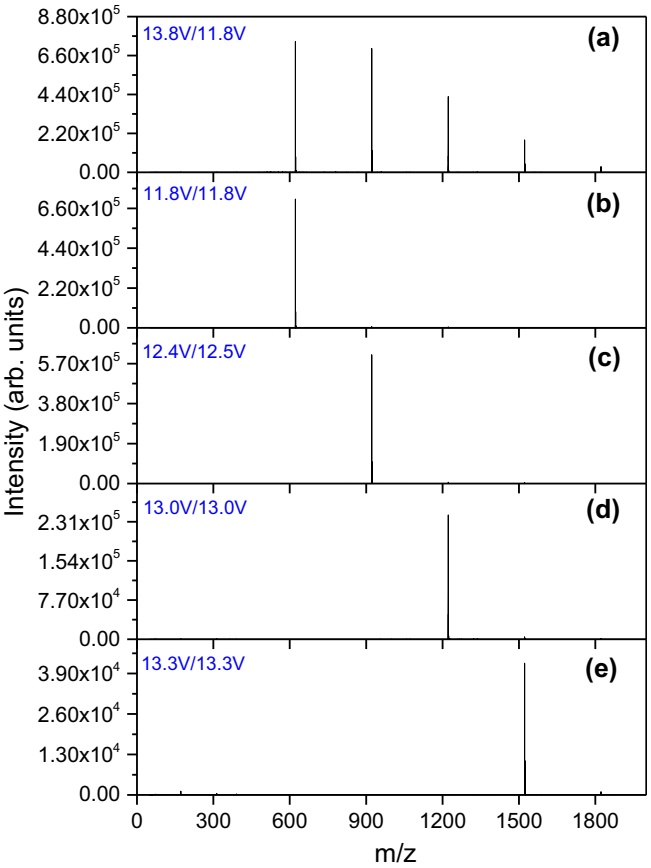

Figure 6. Mass spectra of Agilent tune mixture show the transmission of each ion with negligible loss by maintaining TW1 sequence of 11110000 and TW2 sequence at 10000000 while varying the TW amplitudes. TW1 and TW2 speeds were maintained at 143.56×10^3 mm/s and 22.20×10^3 mm/s, respectively. The legend in the graph indicates TW1 amplitude/TW2 amplitude in V

mobility ions and where the mobility difference is small, transmission is compromised in order to achieve higher resolution filtering.

The effect of varying the applied TW sequence on the filtering capability was also investigated. The sequence of the second section TW2 was systematically varied from 11110000 to 10000000 while maintaining all other parameters constant. Figure 5 shows normalized intensities of the ions associated with each sequence where the data was normalized to the condition where all ions were transmitted (similar to Figure 3d). Here, the change in the TW2 sequence was accompanied by adjusting the TW2 speed in order to maximize the transmission of a specific ion. It is evident that changing the TW2 sequence from 11110000 to 10000000 can improve the signal by reducing the observed ion losses accompanying the filtering process from 53% to 15%, 90% to 45%, and 97% to 62% for *m/z* 922, 1222, and 1522, respectively (Supplementary Information Figure S2). Alternative TW sequences in section 2 enabled a better balance between the selectivity and sensitivity. Figure 6 illustrates a series of filtering experiments where the sequences at TW1 and TW2 were kept at 11110000 and 10000000, respectively, while the TWs amplitudes in the two sections were varied independently. Figure 6a shows the baseline reference mass spectrum and the transmission of all ions in the Agilent tune mixture. Herein, while maintaining the frequencies fixed, the TW1 and TW2 amplitudes were systematically changed to achieve filtering of individual ions (Figures S3, S4). Figure 6 shows that by appropriately choosing the amplitudes of TW1 and TW2 frequencies, selected ions can be efficiently transmitted through the device with minimum ion losses. We also evaluated the SLIM mobility analyzer with a mixture of nine peptides that also produce multiply charged species of more closely spaced mobilities than the singly charged ions from the Agilent tuning mixture. The reduced mobility values for the peptides in the mixture are listed in Table 1. The Figure 7 shows the mobility spectra obtained. The spectra were plotted by replacing the centroid of each *m/z* peak corresponding to the nine peptides by its mobility. Here the filtering was obtained by adjusting the traveling wave amplitude, similar to the experiment in Figure 6. The panel a in Figure 7 corresponds to the full spectrum obtained by keeping the amplitude difference sufficiently large

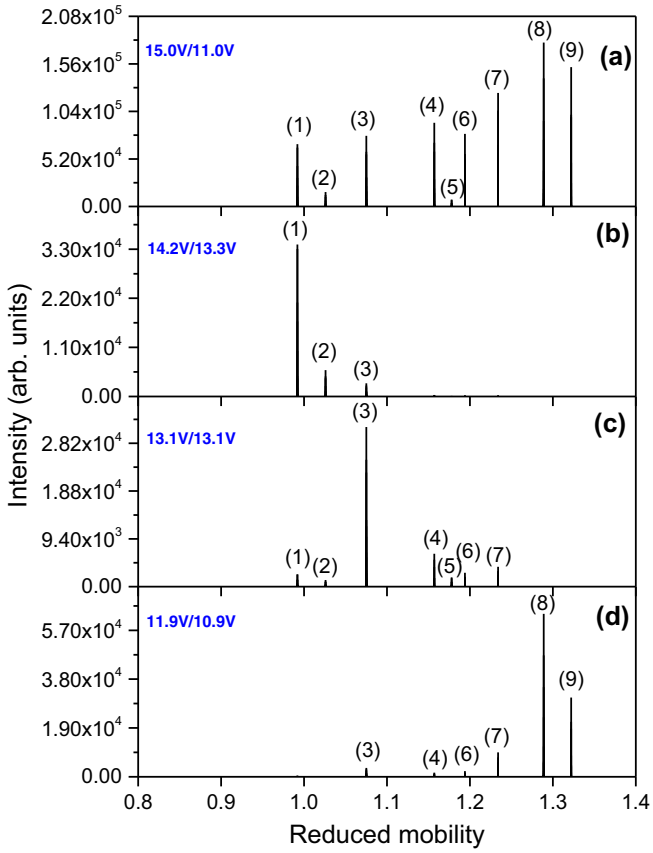

Figure 7. Mobility spectra for a mixture of nine peptides showing the transmission of the device at different settings. TW1 sequence was 11110000 and TW2 sequence was 10000000. Panel **(a)** represents no filtering applied and the transmission of all ions (TW1 and TW2 amplitudes are 15 V and 11 V, respectively). The filtering is achieved by changing the TW1 and TW2 amplitudes (from panel **b** to panel **d**) 14.2 V and 13.3 V, 13.1 V and 13.1 V, 11.9 V and 10.9 V, respectively. TW1 and TW2 frequencies were maintained at 187.96 × 10^3 mm/s and 28.12 × 10^3 mm/s, respectively. The *m/z* and the intensity for few peaks are noted. The peptides used in the mixture are (1) fibrinopeptide A, (2) Substance P, (3) melittin, (4) angiotensin II, (5) renin, (6) bradykinin, (7) H neurotensin, (8) H angiotensin, (9) kemptide

enough to transmit all ions to the mass spectrometer. In panel b, the difference in amplitudes was reduced and adjusted to allow the fibrinopeptide A ions to pass through, but a 50% loss was observed compared with the full spectrum. In panel c, amplitude window was adjusted to allow melittin ions to pass through; in this case a 60% loss was observed. In the panel d, H angiotensin was allowed to pass but in this case also a 60% loss was observed. In this experiment, the resolution was found to be 11.9 for fibrinopeptide A (Figure 7, panel b). Results shown in Figure 7 support that, as expected, the SLIM module functions as an ion mobility filter, not as an *m/z* filter. Although different peptides can be transmitted preferentially, ions of close mobilities are challenging to filter with the current resolution of this initial device configuration.

Conclusion

In this work, we demonstrated a new concept for ion mobility separations in SLIM, which we have initially evaluated using both simulations and experiments. Simulations showed that the filtering effect is a result of the balance between the ion velocity due to TW and the opposing constant DC gradient and applied differently in each of two sections of the SLIM module. In the first section of the device, those ions whose velocities due to the traveling wave are higher than that due to the DC gradient will pass through, whereas in the second section this is reversed. Therefore, ions can be filtered according to their mobilities and the effective low and high mobility cutoffs as they are transported through the device. The effects of different parameters on the efficiency of the device have been experimentally investigated, such as the applied DC gradients along with TW parameters such as speed, sequence, and amplitude. Maintaining the DC gradient, TW amplitude, and sequence fixed in both sections of the device, traveling wave frequencies (i.e., speed) on both the sections could be adjusted to transmit the species of interest. In this case, the TW speed of the second section needs to be higher than that of the first section.

In this initial work, significant ion losses accompanied the filtering process, and these losses were found to be reduced by using a different TW sequence in the second section. The present mobility analyzer provided significantly improved performance when the TW1 sequence of 11110000 and TW2 sequence of 10000000 was applied, while the TW1 and TW2 amplitudes varied simultaneously. These results illustrate the variety of parameters that impact the resolution of the current device. With our current power supply, we can adjust the TW frequency in steps of 1000 Hz (corresponding to 1480 mm/s TW speed) and the TW amplitude in steps of 0.1 V. We anticipate that improved power supplies with a capability to more finely tune the TW frequency and amplitude will enable higher resolution. Efforts are underway to better understand other factors that affect the resolution of the device (such as the length of the device and the number of alternating DC gradient sections used) and to explore alternative designs providing improved performance. We note this initial SLIM mobility filter analyzer works with continuous ion beam resulting in high duty cycle operation providing a basis for the targeted analysis of compounds based upon their mobility and without the need for high electric fields or for pulsed/trapped analyte injection.

Acknowledgments

Portions of this research were supported by the Laboratory Directed Research and Development Program at Pacific Northwest National Laboratory, the National Institute of General Medical Sciences (P41 GM103493). Work was performed at the W. R. Wiley Environmental Molecular Sciences Laboratory (EMSL), a DOE national scientific user facility at the Pacific Northwest National Laboratory (PNNL). PNNL is operated by Battelle for the DOE under contract DE-AC05-76RL0 1830.

References

1. Harper, J.D., Charipar, N.A., Mulligan, C.C., Zhang, X., Cooks, R.G., Ouyang, Z.: Low-temperature plasma probe for ambient desorption ionization. Anal. Chem. **80**, 9097–9104 (2008)
2. Yinon, J.: Field detection and monitoring of explosives. TrAC Trends Anal. Chem. **21**, 292–301 (2002)
3. Hallowell, S.F.: Screening people for illicit substances: a survey of current portal technology. Talanta **54**, 447–458 (2001)
4. Yinon, J.: Forensic and environmental detection of explosives. John Wiley & Son, Chichester (1999)
5. Ewing, R.G., Atkinson, D.A., Eiceman, G., Ewing, G.: A critical review of ion mobility spectrometry for the detection of explosives and explosive related compounds. Talanta. **54**, 515–529 (2001)
6. Armenta, S., Alcala, M., Blanco, M.: A review of recent, unconventional applications of ion mobility spectrometry (IMS). Anal. Chim. Acta. **703**, 114–123 (2011)
7. Kanu, A.B., Dwivedi, P., Tam, M., Matz, L., Hill, H.H.: Ion mobility-mass spectrometry. J.Mass Spectrom. **43**, 1–22 (2008)
8. Cumeras, R., Figueras, E., Davis, C., Baumbach, J.I., Gracia, I.: Review on ion mobility spectrometry. Part 1: Current instrumentation. Analyst. **140**, 1376–1390 (2015)
9. Cumeras, R., Figueras, E., Davis, C., Baumbach, J.I., Gracia, I.: Review on ion mobility spectrometry. Part 2: Hyphenated methods and effects of experimental parameters. Analyst. **140**, 1391–1410 (2015)
10. McLean, J.A., Ruotolo, B.T., Gillig, K.J., Russell, D.H.: Ion mobility-mass spectrometry: a new paradigm for proteomics. Int. J. Mass Spectrom. **240**, 301–315 (2005)
11. Lanucara, F., Holman, S.W., Gray, C.J., Eyers, C.E.: The power of ion mobility-mass spectrometry for structural characterization and the study of conformational dynamics. Nat. Chem. **6**, 281–294 (2014)
12. Ruotolo, B.T., Benesch, J.L., Sandercock, A.M., Hyung, S.-J., Robinson, C.V.: Ion mobility-mass spectrometry analysis of large protein complexes. Nat. Protoc. **3**, 1139 (2008)
13. Michaelevski, I., Kirshenbaum, N., Sharon, M.: T-wave ion mobility-mass spectrometry: basic experimental procedures for protein complex analysis. JoVE (J Visual Exp). **41**, e1985–e1985 (2010)
14. Mesleh, M., Hunter, J., Shvartsburg, A., Schatz, G., Jarrold, M.: Structural information from ion mobility measurements: effects of the long-range potential. J. Phys. Chem. **100**, 16082–16086 (1996)
15. Giles, K., Pringle, S.D., Worthington, K.R., Little, D., Wildgoose, J.L., Bateman, R.H.: Applications of a travelling wave-based radio-frequency-only stacked ring ion guide. Rapid Commun. Mass Spectrom. **18**, 2401–2414 (2004)
16. Guha, S., Li, M., Tarlov, M.J., Zachariah, M.R.: Electrospray-differential mobility analysis of bionanoparticles. Trends Biotechnol. **30**, 291–300 (2012)
17. Michelmann, K., Silveira, J.A., Ridgeway, M.E., Park, M.A.: Fundamentals of trapped ion mobility spectrometry. J. Am. Soc. Mass Spectrom. **26**, 14–24 (2015)
18. Ewing, M.A., Conant, C.R.P., Zucker, S.M., Griffith, K.J., Clemmer, D.E.: Selected overtone mobility spectrometry. Anal. Chem. **87**, 5132–5138 (2015)
19. Zucker, S.M., Ewing, M.A., Clemmer, D.E.: Gridless overtone mobility spectrometry. Anal. Chem. **85**, 10174–10179 (2013)
20. Rus, J., Moro, D., Sillero, J.A., Royuela, J., Casado, A., Estevez-Molinero, F., de la Mora Fernández, J.: IMS-MS studies based on coupling a differential mobility analyzer (DMA) to commercial API-MS systems. Int. J. Mass Spectrom. **298**, 30–40 (2010)
21. Brown, L.J., Creaser, C.S.: Field asymmetric waveform ion mobility spectrometry analysis of proteins and peptides: a review. Curr. Anal. Chem. **9**, 192–198 (2013)
22. Guevremont, R.: High-field asymmetric waveform ion mobility spectrometry: anew tool for mass spectrometry. J. Chromatogr. A. **1058**, 3–19 (2004)
23. Kolakowski, B.M., Mester, Z.: Review of applications of high-field asymmetric waveform ion mobility spectrometry (FAIMS) and differential mobility spectrometry (DMS). Analyst. **132**, 842–864 (2007)
24. Vidal-de-Miguel, G., Macía, M., Cuevas, J.: Transversal modulation ion mobility spectrometry (TM-IMS), a new mobility filter overcoming turbulence related limitations. Anal. Chem. **84**, 7831–7837 (2012)
25. Giles, K., Wildgoose, J.L., Langridge, D.J., Campuzano, I.: A method for direct measurement of ion mobilities using a traveling wave ion guide. Int. J. Mass Spectrom. **298**, 10–16 (2010)
26. Giles, K., Williams, J.P., Campuzano, I.: Enhancements in traveling wave ion mobility resolution. Rapid Commun. Mass Spectrom. **25**, 1559–1566 (2011)
27. Ibrahim, Y.M., Hamid, A.M., Deng, L., Garimella, S.V., Webb, I.K., Baker, E.S., Smith, R.D.: New frontiers for mass spectrometry based upon structures for lossless ion manipulations. Analyst. **142**, 1010–1021 (2017)
28. Chen, T.-C., Ibrahim, Y.M., Webb, I.K., Garimella, S.V., Zhang, X., Hamid, A.M., Deng, L., Karnesky, W.E., Prost, S.A., Sandoval, J.A., Norheim, R.V., Anderson, G.A., Tolmachev, A.V., Baker, E.S., Smith, R.D.: Mobility-selected ion trapping and enrichment using structures for lossless ion manipulations. Anal. Chem. (2016)
29. Deng, L., Ibrahim, Y.M., Baker, E.S., Aly, N.A., Hamid, A.M., Zhang, X., Zheng, X., Garimella, S.V., Webb, I.K., Prost, S.A., Sandoval, J.A., Norheim, R.V., Anderson, G.A., Tolmachev, A.V., Smith, R.D.: Ion mobility separations of isomers based upon long path length structures for lossless ion manipulations combined with mass spectrometry. ChemistrySelect. **1**, 2396–2399 (2016)
30. Deng, L., Ibrahim, Y.M., Hamid, A.M., Garimella, S.V., Webb, I.K., Zheng, X., Prost, S.A., Sandoval, J.A., Norheim, R.V., Anderson, G.A., Tolmachev, A.V., Baker, E.S., Smith, R.D.: Ultra-high resolution ion mobility separations utilizing traveling waves in a 13-m serpentine path length structures for lossless ion manipulations module. Anal. Chem. **88**, 8957–8964 (2016)
31. Hamid, A.M., Ibrahim, Y.M., Garimella, S.V., Webb, I.K., Deng, L., Chen, T.-C., Anderson, G.A., Prost, S.A., Norheim, R.V., Tolmachev, A.V., Smith, R.D.: Characterization of traveling wave ion mobility separations in structures for lossless ion manipulations. Anal. Chem. **87**, 11301–11308 (2015)
32. Webb, I.K., Garimella, S.V., Norheim, R.V., Baker, E.S., Ibrahim, Y.M., Smith, R.D.: A structures for lossless ion manipulations (SLIM) module for collision induced dissociation. J. Am. Soc. Mass Spectrom. **27**, 1–4 (2016)
33. Webb, I.K., Garimella, S.V.B., Tolmachev, A.V., Chen, T.-C., Zhang, X., Cox, J.T., Norheim, R.V., Prost, S.A., LaMarche, B., Anderson, G.A., Ibrahim, Y.M., Smith, R.D.: Mobility-resolved ion selection in uniform drift field ion mobility spectrometry/mass spectrometry: dynamic switching in structures for lossless ion manipulations. Anal. Chem. **86**, 9632–9637 (2014)
34. Webb, I.K., Garimella, S.V.B., Tolmachev, A.V., Chen, T.-C., Zhang, X., Norheim, R.V., Prost, S.A., LaMarche, B., Anderson, G.A., Ibrahim, Y.M., Smith, R.D.: Experimental evaluation and optimization of structures for lossless ion manipulations for ion mobility spectrometry with time-of-flight mass spectrometry. Anal. Chem. **86**, 9169–9176 (2014)
35. Zhang, X., Garimella, S.V.B., Prost, S.A., Webb, I.K., Chen, T.-C., Tang, K., Tolmachev, A.V., Norheim, R.V., Baker, E.S., Anderson, G.A., Ibrahim, Y.M., Smith, R.D.: Ion trapping, storage, and ejection in structures for lossless ion manipulations. Anal. Chem. **87**, 6010–6016 (2015)
36. Tolmachev, A.V., Webb, I.K., Ibrahim, Y.M., Garimella, S.V.B., Zhang, X., Anderson, G.A., Smith, R.D.: Characterization of ion dynamics in structures for lossless ion manipulations. Anal. Chem. **86**, 9162–9168 (2014)
37. Kimmel, J.R., Engelke, F., Zare, R.N.: Novel method for the production of finely spaced Bradbury-Nielson gates. Rev. Sci. Instrum. **72**, 4354–4357 (2001)
38. Ibrahim, Y., Belov, M.E., Tolmachev, A.V., Prior, D.C., Smith, R.D.: Ion funnel trap interface for orthogonal time-of-flight mass spectrometry. Anal. Chem. **79**, 7845–7852 (2007)
39. Kelly, R.T., Tolmachev, A.V., Page, J.S., Tang, K., Smith, R.D.: The ion funnel: theory, implementations, and applications. Mass Spectrom. Rev. **29**, 294–312 (2010)
40. Deng, L., Garimella, S.V., Hamid, A.M., Webb, I.K., Attah, I.K., Norheim, R.V., Prost, S.A., Zheng, X., Sandoval, J.A., Baker, E.S.: Compression ratio ion mobility programming (CRIMP) accumulation and compression of billions of ions for ion mobility-mass spectrometry using traveling waves in structures for lossless ion manipulations (SLIM). Anal. Chem. **89**, 6432 (2017)
41. Zakett, D., Flynn, R., Cooks, R.: Chlorine isotope effects in mass spectrometry by multiple reaction monitoring. J. Phys. Chem. (United States) **82**, 2359–2362 (1978)

42. Liebler, D.C., Zimmerman, L.J.: Targeted quantitation of proteins by mass spectrometry. Biochemistry. **52**, 3797 (2013)
43. SIMION8.0/8.1 User manual
44. Appelhans, A.D., Dahl, D.A.: SIMION ion optics simulations at atmospheric pressure. Int. J. Mass Spectrom. **244**, 1–14 (2005)
45. Shvartsburg, A.A., Creese, A.J., Smith, R.D., Cooper, H.J.: Separation of peptide isomers with variant modified sites by high-resolution differential ion mobility spectrometry. Anal. Chem. **82**, 8327–8334 (2010)